Atmospheric semidiurnal lunar tide climatology simulated by the Whole Atmosphere Community Climate Model

N. M. Pedatella,[1] H.-L. Liu,[1] and A. D. Richmond[1]

Received 3 April 2012; revised 4 May 2012; accepted 22 May 2012; published 30 June 2012.

[1] The atmospheric semidiurnal lunar tide is added to the Whole Atmosphere Community Climate Model (WACCM) through inclusion of an additional forcing mechanism. The simulated climatology of the semidiurnal lunar tide in surface pressure and zonal and meridional winds in the mesosphere and lower thermosphere (MLT) is presented. Prior observations and modeling results demonstrate characteristic seasonal and latitudinal variability of the semidiurnal lunar tide in surface pressure, and the WACCM reproduces these features. In the MLT, the WACCM simulations reveal a primarily semiannual variation with maxima near December and June solstice. The peak amplitudes in the MLT zonal and meridional winds are $\sim$5–10 ms^{-1}, and occur at mid to high latitudes in the summer hemisphere. We have further compared the WACCM simulation results in the MLT with those from the Global Scale Wave Model (GSWM). The overall latitude and seasonal variations are consistent between these two models. However, the GSWM peak amplitudes are $\sim$2–3 times larger than those in the WACCM. This is thought to be related to deficiencies in the GSWM and not the WACCM simulations. With the exception of smaller amplitudes during Northern Hemisphere summer months, the WACCM simulations of the semidiurnal lunar tide in the MLT are also shown to be generally consistent with prior observations and modeling results. The reduced amplitudes in the WACCM simulations during Northern Hemisphere summer months are thought to be related to the influence of the cold-pole bias in WACCM on the propagation of the lunar tide during these months.

Citation: Pedatella, N. M., H.-L. Liu, and A. D. Richmond (2012), Atmospheric semidiurnal lunar tide climatology simulated by the Whole Atmosphere Community Climate Model, *J. Geophys. Res.*, *117*, A06327, doi:10.1029/2012JA017792.

1. Introduction

[2] The atmospheric lunar tide arises due to the gravitational forcing of the moon on the combined Earth-ocean-atmosphere system. In addition to gravitational forcing of the atmosphere directly, the lunar tide in the atmosphere is driven by the tidally induced movement of the solid Earth and oceans as well as the redistribution of mass associated with these motions. Orbital variations result in the excitation of several periodicities that are associated with the gravitationally driven lunar tide [e.g., *Chapman and Lindzen*, 1970]. The atmospheric response to the vast majority of the possible lunar tidal periods is relatively small, and the most prominent period of oscillation is by far the semidiurnal lunar tide. The semidiurnal lunar tide occurs at a period of $\sim$12.42 solar hours, and is commonly referred to as the M2 tide. Despite being considerably smaller than the solar driven tides, the M2 tide has been studied for well over a century in numerous atmospheric observations as well as theoretical models. The primary reason that the lunar tide has attracted considerable attention is due to the fact that, at least in principle, the tidal forcing is extremely well known. Thus, by studying, for example, seasonal variations in the atmospheric lunar tide it is possible to infer the atmospheric changes (i.e. temperatures and winds) that must occur in order to generate the observed lunar tide variability.

[3] Early studies of the atmospheric lunar tide focused on surface pressure observations. Many early studies suffered from insufficient observations, and the atmospheric lunar tide was first reliably determined in the mid nineteenth century by *Sabine* [1847]. *Sabine* [1847] clearly showed the dominance of the semidiurnal lunar tide, along with its tendency to maximize near lunar upper and lower transit (i.e., lunar local times of noon and midnight). Given the extensive history of surface pressure observations of the lunar tide, we will only briefly summarize its salient characteristics. The semidiurnal lunar tide in surface pressure exhibits clear latitudinal and seasonal dependencies. In particular, it achieves largest amplitudes in the equatorial region during Northern Hemisphere summer months. A significant reduction in the amplitude and decrease in phase (i.e. maximum occurs at a later lunar time) is known to occur around December solstice [*Chapman and Tschu*, 1948]. The semidiurnal lunar tide also

[1]High Altitude Observatory, National Center for Atmospheric Research, Boulder, Colorado, USA.

Corresponding author: N. M. Pedatella, High Altitude Observatory, National Center for Atmospheric Research, PO Box 3000, Boulder, CO 80307-3000, USA. (nickp@ucar.edu)

0148-0227/12/2012JA017792

exhibits a slight hemispheric asymmetry, with larger amplitudes and phases occurring in the Southern Hemisphere [*Haurwitz and Cowley*, 1969]. The semidiurnal lunar tide is dominated by its migrating (i.e. longitude invariant) component. However, nonmigrating lunar tides are also present, and these generate a longitudinal variability in the semidiurnal lunar tide that is most pronounced in the equatorial region. We note that these are only the most prominent features of the semidiurnal lunar tide in surface pressure, and the interested reader is referred to the work by *Chapman and Lindzen* [1970] for a more comprehensive discussion.

[4] Similar to solar-thermal tides that are generated by infrared absorption and latent heat release in the tropical troposphere [e.g., *Hagan and Forbes*, 2002], the semidiurnal lunar tide propagates vertically, achieving large amplitudes around 90–120 km in the mesosphere and lower thermosphere (MLT). Near ~90–100 km, ground-based radar observations of the semidiurnal lunar tide reveal that it achieves amplitudes of ~5–10 ms^{-1} [*Tsuda et al.*, 1981; *Stening et al.*, 1987; *Stening and Vincent*, 1989; *Stening et al.*, 1994; *Stening and Jacobi*, 2001; *Stening et al.*, 2003; *Sandford et al.*, 2006]. These studies have revealed a distinct seasonal behavior to the semidiurnal lunar tide in the MLT with maximum amplitudes generally occurring around December solstice and also between July and September. Through comparison of radar observations in the Northern and Southern Hemispheres, *Stening et al.* [1994] investigated the large-scale latitudinal structure of the semidiurnal lunar tide, and found that it is latitudinally symmetric during solstice months and asymmetric around equinox. Despite these past studies, current understanding of the semidiurnal lunar tide in the MLT remains extremely limited. This is primarily due to the fact that extended observations are necessary in order to reliably extract the semidiurnal lunar tide. Extended observations are required owing to the significantly smaller amplitude of the semidiurnal lunar tide compared to the semidiurnal solar tide combined with the similar frequency of the solar and lunar semidiurnal tides. Accurate determination of the climatological behavior of the semidiurnal lunar tide in the MLT is further complicated by the significant inter-annual variability that has been observed [e.g., *Stening et al.*, 1994].

[5] The semidiurnal atmospheric lunar tide has also been extensively investigated through numerical modeling [*Geller*, 1970; *Hollingsworth*, 1971; *Lindzen and Hong*, 1974; *Aso et al.*, 1981; *Forbes*, 1982a, 1982b; *Vial and Forbes*, 1994]. These studies have focused on the importance of different forcing mechanisms for generating the atmospheric lunar tide [e.g., *Hollingsworth*, 1971], and also on the importance of the background atmospheric winds and temperatures on the propagation of the lunar tide into the MLT [*Lindzen and Hong*, 1974; *Aso et al.*, 1981]. Numerical models of the atmospheric lunar tide have implemented the lunar tidal forcing with varying degrees of complexity, with the most comprehensive forcing being that used by *Vial and Forbes* [1994]. *Vial and Forbes* [1994] accounted for lunar tidal forcing due to the Earth and ocean tides, along with the effects of the ocean load tide. Owing to the aforementioned difficulty and sparseness of lunar tidal observations in the MLT, numerical models are particularly useful for investigating the lunar tide in the MLT, and this has been the primary focus of the majority of the past efforts to model the atmospheric lunar tide.

[6] Prior numerical modeling studies have made use of linearized, steady state models that rely on a specified zonal mean background atmosphere structure. While such an approach is useful for investigating the general behavior of the semidiurnal lunar tide, it can be considered to be limited due to the significant dependence of the lunar tide on the specified background atmosphere. In the present study, we add a lunar tidal forcing to the Whole Atmosphere Community Climate Model (WACCM) and investigate the climatological behavior of the semidiurnal lunar tide. The WACCM is a non-linear, chaotic (i.e. exponential growth of initial error) model and it thus provides the opportunity to study the semidiurnal lunar tide under presumably more realistic atmospheric conditions. Investigating the lunar tide in a model such as the WACCM additionally provides the opportunity to elucidate potential short-term variability in the semidiurnal lunar tide. While the present study focuses on establishing the climatological behavior of the lunar tide in the WACCM, a follow-on study (N. M. Pedatella et al., Simulations of solar and lunar tidal variability in the mesosphere and lower thermosphere during sudden stratospheric warmings and their influence on the low-latitude ionosphere, submitted to *Journal of Geophysical Research*, 2012) investigates short-term variability of the lunar tide in the WACCM during sudden stratospheric warmings (SSWs), and whether this variability significantly influences the low-latitude ionosphere during SSWs as has been suggested by several recent studies [e.g., *Fejer et al.*, 2010; *Park et al.*, 2012; *Yamazaki et al.*, 2012].

2. Numerical Models

2.1. Whole Atmosphere Community Climate Model (WACCM)

[7] The WACCM is the vertical extension of the National Center for Atmospheric Research Community Atmosphere Model (CAM) into the lower thermosphere. A detailed description of the WACCM is provided by *Garcia et al.* [2007] and not repeated herein. The specific details of the simulation performed as part of the present study are as follows. Solar maximum ($f10.7 = 210 \times 10^{-22} Wm^{-2}Hz^{-1}$) and moderate geomagnetic activity ($K_p = 4$) conditions are used. The model resolution is 1.9° in latitude and 2.5° in longitude. The simulations are performed using prescribed oceans and ice. The atmospheric lunar tide is sensitive to the winds and temperatures throughout the atmosphere, and the large scale atmospheric variability that is present in the WACCM can introduce significant short-term and inter-annual variability in the lunar tide. Therefore, in order to establish the climatological behavior of the lunar tide, we have performed a 10-year perpetual simulation of the WACCM. All of the results in the present paper are based on the analysis of hourly model results (see section 3.1), and averaged over the entire 10-year simulation. The results are thus representative of the climatology of the semidiurnal atmospheric lunar tide.

2.2. Implementation of the Lunar Tide

[8] To implement the atmospheric lunar tide in the WACCM, we add an additional forcing term to the zonal and meridional momentum equations. We incorporate effects due to the M2 lunar potential, the Earth tide, and the

migrating semidiurnal lunar ocean tide. The additional forcing we consider is the horizontal gradient of the tidal potential, on constant pressure surfaces, due to the sum of the M2 lunar potential (Ω_{M2}), the geopotential change from the solid Earth's mass redistribution (Ω_e), and the potential change from vertical displacement of the Earth/ocean surface in the Earth's gravitational field [$(\zeta_e + \zeta_o)g$, where ζ_e is the solid Earth surface displacement, ζ_o is the ocean tidal height with respect to the solid Earth surface, and g is the acceleration of gravity]. We neglect the considerably smaller effects on the potential due to ocean-mass redistribution and the ocean load tide on the solid earth [see, for example, *Vial and Forbes*, 1994]. The potential is thus $\Omega = \Omega_{M2} + \Omega_e + (\zeta_e + \zeta_o)g$. The M2 lunar potential is well known [e.g., *Chapman and Lindzen*, 1970] , and is given by

$$\Omega_{M2} = -0.7933\left(\frac{h + r_o}{r_o}\right)^2 P_2^2(\theta)\cos(2\tau) \quad (1)$$

where h is altitude, r_o is the radius of the Earth, $P_2^2(\theta)$ (= $3\sin^2(\theta)$) is the associated Legendre polynomial, θ is colatitude, and τ is the lunar local time in radians. The units of equation (1) are m^2s^{-2}. The solid Earth tide produces a simple multiplicative modification of the potential. At the Earth's surface, $\Omega_e = k_2\Omega_{M2}$, where $k_2 = 0.302$ is a Love number [*Vial and Forbes*, 1994]. We neglect height variations of Ω_e. The solid-Earth surface displacement is also proportional to Ω_{M2}, such that $\zeta_e g = -h_2\Omega_{M2}$, where $h_2 = 0.609$ is another Love number. Comprehensive treatment of the ocean tides are complicated by the large number of tidal components that are generated by coastal regions. For the ocean tide, we have chosen to neglect the longitudinal variability, and have only included the term of the migrating semidiurnal lunar ocean tide that is proportional to $P_2^2(\theta)$. We have neglected additional ocean tide forcing terms in order to simplify the implementation of the forcing in the WACCM. Amplitude and phase values given by *Ray* [1999] are used for the ocean tide. Note that although the phase of the M2 lunar potential and solid Earth tide are 180° (i.e., they minimize at lunar local times of noon and midnight), the phase of the migrating P_2^2 component of the ocean tide is ~130°. The amplitude of $\zeta_o g$ of the migrating P_2^2 component of the ocean tide is 9.81 ms^{-2} × 0.0323 m = 0.317 m^2s^{-2}. Adding the components of Ω at the Earth's surface results in a net potential of

$$\Omega = 0.788P_2^2(\theta)\cos(2\tau - 162.2°) \quad (2)$$

Our neglect of the components of the ocean tide other than the migrating P_2^2 term, and our neglect of the load tide obviously represents a simplification to the real forcing of the atmosphere. Nonetheless, the forcing we implement incorporates the dominate forcing mechanisms, and, as will be shown in section 3, we are able to capture the salient large-scale features of the semidiurnal lunar tide in the atmosphere. While we recognize that our approach has its shortcomings, our ability to reproduce the general climatological behavior of the semidiurnal lunar tide in the atmosphere serves to validate the efficacy of our method for implementing the lunar tide in the WACCM.

2.3. Global Scale Wave Model

[9] In addition to comparing with observations, we validate the semidiurnal migrating lunar tide simulated by the WACCM in the MLT through comparison with results from the Global Scale Wave Model (GSWM). This permits a global comparison of the lunar tide in the MLT which would not be possible through comparison with observations alone. The GSWM is a linear, two-dimensional tidal model that extends from the surface to the thermosphere. The GSWM solves the linearized equations of motion based on a specified zonal mean background atmosphere. Specific details regarding the numerics of the GSWM can be found in *Hagan et al.* [1993, 1995, 1999]. For the present study, the tidal forcing applied to the GSWM is only due to the lunar tide, and we calculate the tidal response at the lunar semidiurnal period of 12.42 h. The semidiurnal lunar tide in the GSWM is implemented by adding an additional forcing term to the momentum equations that is similar to what is used in the WACCM. For the present study, we replace the background atmosphere zonal mean densities, temperatures and zonal winds used in the GSWM with monthly average values from the WACCM. This allows for a more direct comparison between the lunar tides in the GSWM and those simulated by the WACCM. Despite the similar forcing and background atmospheres, differences in the lunar tide simulated by these two models is to be expected due to several significant differences between the GSWM and WACCM. Perhaps most important is the different treatment of gravity waves and dissipation in the MLT. The WACCM incorporates a comprehensive treatment of gravity waves, while the GSWM uses an effective Rayleigh friction for gravity wave drag. This is a considerable difference, and may lead to discrepancies in the simulated lunar tides. Additionally, the WACCM is a nonlinear model, and the lunar tide simulated in the WACCM can thus be impacted by nonlinear interactions with other waves. Such interactions are absent from a linear model, such as the GSWM, and this may result in further differences between the lunar tide simulated by the GSWM and the WACCM.

3. Results and Discussion

3.1. Estimation of Semidiurnal Lunar Tide

[10] Throughout the following we present results for the semidiurnal lunar tide that are based on least squares fitting of the WACCM simulation results. Hourly output fields (e.g., surface pressures, winds, temperatures) at each latitude and height are used to extract the components of the solar and lunar tides by performing a least squares fit of the form

$$\bar{A} + \sum_{n=1}^{3}\sum_{s=n-5}^{n+5} A_{n,s}\cos\left(n\Omega t + s\lambda - \phi_{n,s}\right) + \sum_{s=-3}^{7} L_s\cos(2\tau + (s-2)\lambda - \Phi_s) \quad (3)$$

where t is universal time in hours, Ω is the rotation rate of the Earth, λ is longitude, and τ is lunar local time (in radians). n and s represent the harmonics of a solar day and zonal wave number, respectively. From equation (3), we estimate the parameters $\bar{A}$, $A_{n,s}$, $\phi_{n,s}$, L_s, and Φ_s which represent the mean value, amplitude and phase of the solar tides, and the amplitude and phase of the semidiurnal lunar tide, respectively. The range of zonal wave numbers, s, in equation (3) was chosen to include the range of nonmigrating tides that

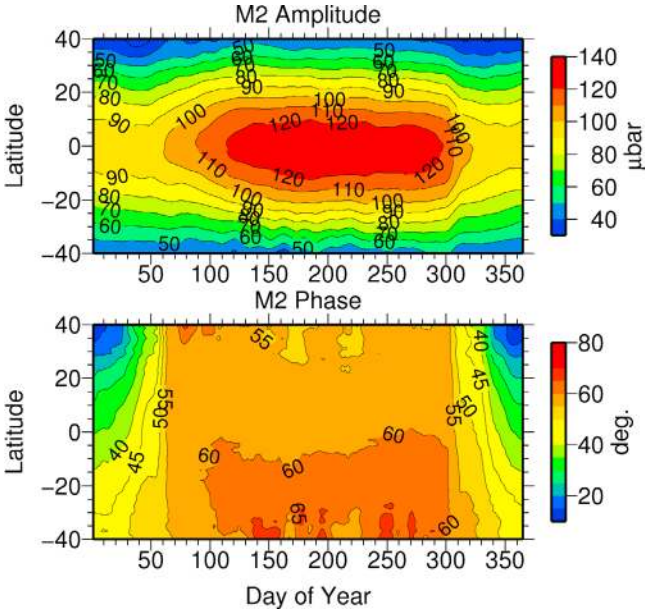

Figure 1. Seasonal and latitudinal variability of the migrating semidiurnal lunar tide (top) amplitude and (bottom) phase in surface pressure.

are considered relevant for capturing the salient features of the solar and lunar variability in space and time. We have not included a linear trend term in equation (3); however, over the time period of the least squares fit (14.75 days), any linear trend will be relatively small, and neglecting this term should not have any significant impact on the estimate of the amplitude and phase of the tides. Note that we estimate the amplitudes and phases for both migrating and nonmigrating components of the diurnal, semidiurnal, and terdiurnal solar tides, but only estimate the semidiurnal lunar tide. Although there may be a small diurnal lunar tidal component, it is anticipated to be significantly smaller than the semidiurnal lunar tide [e.g., *Chapman and Lindzen*, 1970], and it is thus neglected in the present analysis. The amplitudes and phases of the various solar and lunar tides are estimated daily using a moving 14.75 day (approximately half of a lunar month) window. The moving window is necessary to ensure that the fit is performed over an adequate range of lunar local times. The yearly climatology is obtained by vector averaging the various tidal components for each day of the year.

3.2. Surface Pressure Climatology

[11] Given that there is a rich history of both observations and numerical modeling results of the semidiurnal lunar tide in surface pressure, we first present the WACCM climatology of the semidiurnal lunar tide in surface pressure. The seasonal and latitudinal variability of the migrating semidiurnal lunar tide in surface pressure is shown in Figure 1. Note that in Figure 1, and subsequent figures regarding surface pressure, we present the phase results in a manner that is consistent with that used in prior studies of surface pressure observations [e.g., *Haurwitz and Cowley*, 1969]. *Haurwitz and Cowley* [1969] define the semidiurnal lunar tide as $l_2 \sin(2\tau + \lambda_2)$. To compare with prior results, the phases shown in Figures 1 and 2 are for λ_2 ($= -\Phi_s + 90°$), and are thus a modification of the phase, Φ_s, as defined in equation (3). Figure 1 illustrates that the lunar tide amplitude maximizes in the equatorial region. At low-mid latitudes, the amplitude of the lunar tide displays a distinct annual variation with maximum values of ~120−130 μbar occurring between July and September. The phase of the lunar tide is generally constant throughout most of the year, with the exception being a large phase change that occurs between November and February. Figure 1 also reveals a hemispheric asymmetry with slightly larger amplitudes and phases occurring in the Southern Hemisphere.

[12] To more clearly illustrate the hemispheric asymmetry and seasonal variability, Figure 2 shows the amplitude and phase of the migrating semidiurnal lunar tide at 10°N and 10°S latitude. From Figure 2 it can be seen that the amplitude asymmetry is most prevalent during Northern Hemisphere summer months. During this time the amplitude in the Southern Hemisphere is ~5 μbar larger than the Northern Hemisphere amplitude. The large phase change during November to February is again apparent in Figure 2, and it can also be seen that the phase is larger (i.e. the maximum occurs at an earlier lunar time) in the Southern Hemisphere throughout the year.

[13] The longitude and latitude variability of the semidiurnal lunar tide amplitude is shown in Figures 3a–3d for the months of March, July, September, and December, respectively. The results in Figure 3 are for the average of the entire month. Despite the longitude independent forcing of the lunar tide in the WACCM simulations, it is clear from Figure 3 that the WACCM produces longitudinal variability in the lunar tide. The longitude variability is most pronounced at low-latitudes. While we do not suggest that the longitude variability of the lunar tide shown in Figure 3 is wholly representative of the actual nature of the longitude variations, these results indicate that longitudinal variability in the lunar tide can arise due to processes other than

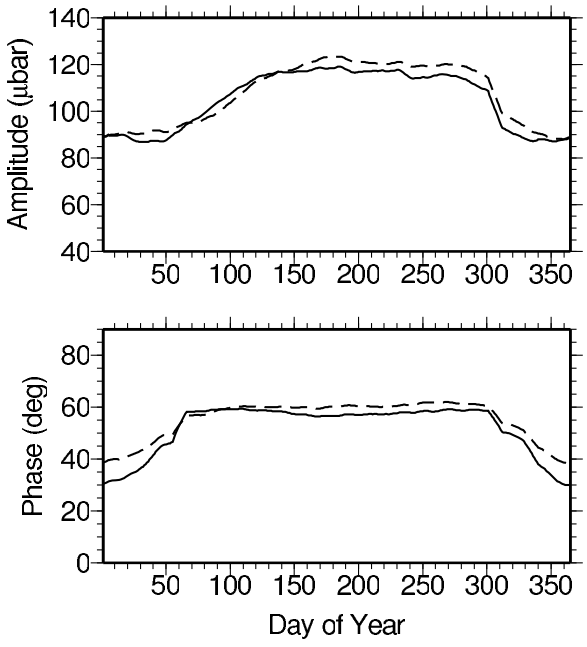

Figure 2. Surface pressure variations of the migrating lunar semidiurnal tide (top) amplitude and (bottom) phase at 10°N (solid) and 10°S (dashed) latitude.

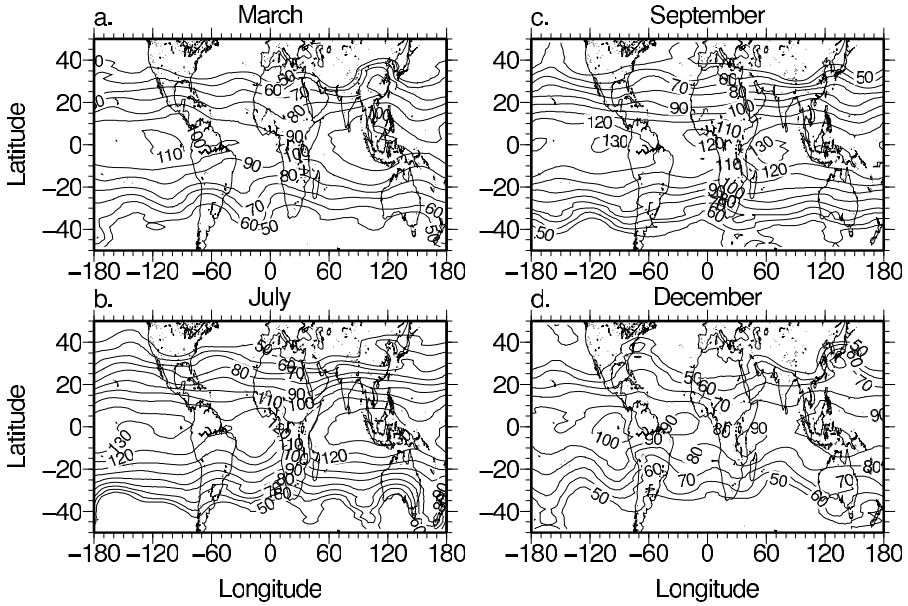

Figure 3. Monthly average latitude and longitude variability of the semidiurnal lunar tide amplitude (in μbar) in surface pressure for (a) March, (b) July, (c) September, and (d) December. Results are based on the semidiurnal migrating lunar tide and nonmigrating tides with zonal wave numbers from $s = -3$ to $s = 7$.

longitude variability in the forcing due to the ocean tide. We consider several potential mechanisms for excitation of the nonmigrating lunar tides that lead to the longitudinal variability in the WACCM. First, it is possible that the lunar tide interacts with topographical features leading to its longitudinal variability. Another possibility is the interaction between the migrating lunar semidiurnal tide and stationary planetary waves. Such interactions are considered likely to take place in a nonlinear model such as the WACCM, and would generate nonmigrating semidiurnal lunar tides. The actual longitudinal variability in the semidiurnal lunar tide is likely to be due to a combination of these effects, which would produce the variations in Figure 3, along with the geographical differences in the forcing of the lunar tide over land and oceans. Note that since we only incorporate forcing due to the migrating semidiurnal lunar tide, the impact of geographical differences in the forcing of the lunar tide are absent from our simulation results. Thus the longitude variability in Figure 3 should not be viewed as entirely representative of the actual lunar tide longitude variability.

[14] It is worthwhile to briefly discuss how the results in Figures 1–3 compare with past observations and modeling results. The seasonal and latitudinal variability in the amplitude of the semidiurnal lunar tide are in good agreement with prior observational results. In particular, our results reproduce the observed amplitude maxima at low-latitudes during Northern Hemisphere summer months as well as the hemispheric asymmetry [e.g., *Haurwitz and Cowley*, 1969]. In the equatorial region, the amplitude maximum of $\sim$120$-$130 μbar and minimum of $\sim$90 μbar is also generally consistent with the observed climatology of the semidiurnal lunar tide. The WACCM simulations capture the large change in phase that occurs around the December solstice as well as the slightly more advanced phase in the Southern Hemisphere. However, the simulated phases tend to be slightly below what is seen in observations. At low-latitudes, the results of *Haurwitz and Cowley* [1969] show phases of $\sim$40$-$60° around December solstice and an annual mean value of $\sim$60$-$80°. Our phase results thus tend to be slightly smaller than what is seen in the observations. The reason for this discrepancy is not known; however, we should note that the observations of phase at low-latitudes show significant variability and we may therefore consider our results to be in reasonably good agreement with the observations.

[15] The most recent comprehensive model of atmospheric lunar tides is that of *Vial and Forbes* [1994], and our results for the semidiurnal lunar tide are in good agreement with their model. Our Figure 2 shows remarkably similar behavior as Figure 1 of *Vial and Forbes* [1994] for the semidiurnal lunar tide at 10°N and 10°S. While the WACCM well reproduces the seasonal and hemispheric differences, there are some differences in the absolute amplitudes and phases. The WACCM amplitudes are $\sim$20$-$30 μbar larger and the phases $\sim$20$-$30° smaller than those of *Vial and Forbes* [1994]. These differences may be related to the more comprehensive forcing model and/or the assumed background atmosphere used in the model of *Vial and Forbes* [1994]. Interestingly, Figure 3b shows equatorial maxima near $\sim$60$-$120°E, 180°E, 100–120°W, and 0–30°W longitude which are similar to the location of the equatorial maxima simulated by *Vial and Forbes* [1994]. Though we do not expect to fully reproduce the longitudinal variability due our neglect of the ocean tide longitude variability, this similarity is encouraging and illustrates that our simulations are able to reasonably reproduce the climatological behavior of the semidiurnal lunar tide in surface pressure.

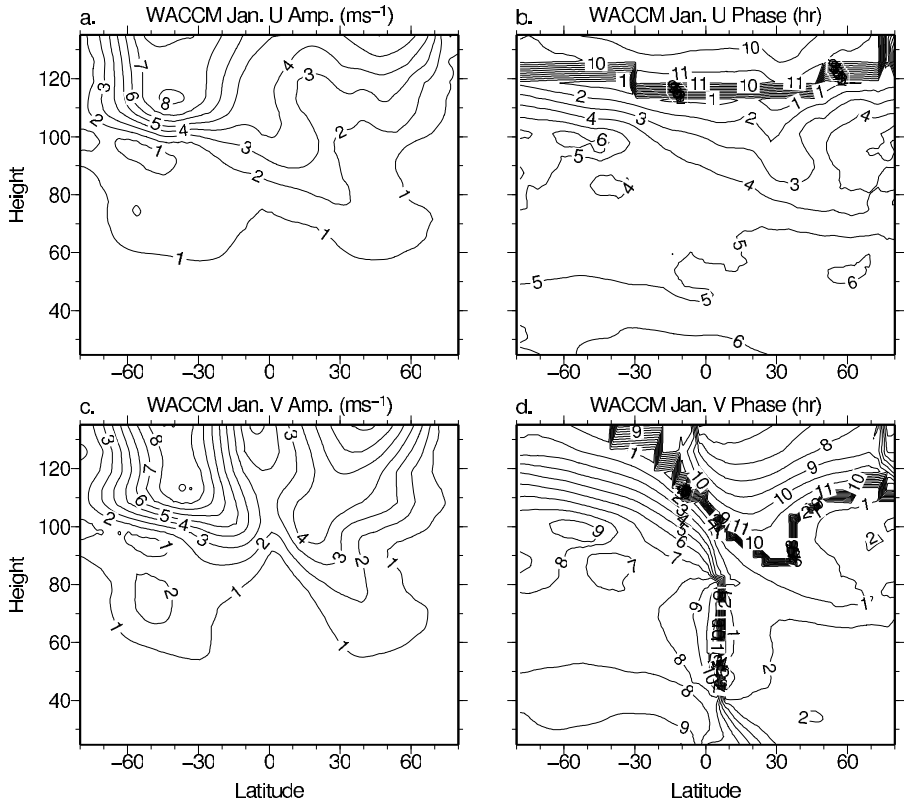

Figure 4. Migrating semidiurnal lunar tide (a) amplitude in zonal neutral wind, (b) phase in zonal neutral wind, (c) amplitude in meridional neutral wind, and (d) phase in meridional neutral wind. Results are for WACCM simulations during January.

3.3. Climatology in the Mesosphere and Lower Thermosphere

[16] The results presented in the prior section illustrate that the WACCM adequately reproduces the semidiurnal lunar tide in surface pressure, and we now turn our attention to the semidiurnal lunar tide in the MLT. The WACCM monthly mean amplitudes and phases of the migrating semidiurnal lunar tide in zonal and meridional winds for January and July are shown in Figures 4 and 6, respectively. Figures 5 and 7 are the corresponding figures based on the GSWM. Focusing first on the WACCM results, it is clear that there exists a significant latitude and seasonal variability in the MLT. During both January and July, the largest amplitudes in both hemispheres occur around 40–50° latitude. Although the amplitudes tend to be slightly larger in the Southern Hemisphere, the phase structure of the lunar tide during January reveals that the lunar tide is predominately symmetric about the equator during this month. The symmetric behavior of the lunar tide in the MLT is to be expected since the forcing is symmetric and the (2, 2) Hough mode is generally the dominant Hough mode of the lunar semidiurnal tide [e.g., *Chapman and Lindzen*, 1970; *Forbes*, 1982b]. During July, the anticipated symmetric nature of the semidiurnal lunar tide is not immediately apparent. This may be due to the zonal mean winds in July generating large asymmetric modes of the semidiurnal lunar tide. The phase observations further reveal that the vertical wavelength of the lunar tide is ~40–50 km in the MLT. During both January and July, the semidiurnal lunar tide amplitudes are hemispherically asymmetric, with the greatest amplitudes occurring in the summer hemisphere. The maximum amplitudes are similar in January and July; however, there is a significant seasonal difference in the amplitude and height of the peak in the winter hemisphere. This is particularly apparent during July in the Southern Hemisphere. As will be discussed in more detail below, we believe that this may be related to problems with the climatological behavior of zonal mean winds and temperatures in the Southern Hemisphere stratosphere at this time.

[17] The general structure of the lunar tide in the GSWM for January (Figure 5), and July (Figure 7) is similar to the WACCM results. This correspondence is to be expected since the propagation of the lunar tide into the MLT is dependent on the background atmosphere, and we have replaced the GSWM background zonal mean densities, temperatures, and zonal winds with those from our WACCM simulations. There are some notable differences between the lunar tide in the WACCM and the GSWM. The most notable difference is that the GSWM amplitudes continue to grow above 110 km, and peak around 120 km with values that are ~2–3 times larger than those in the WACCM simulation. The GSWM and WACCM amplitudes are generally similar up to ~110 km, and the large difference above this altitude could be related to greater effective dissipation in the WACCM above this altitude. The amplitude of the WACCM results are, however, in good agreement

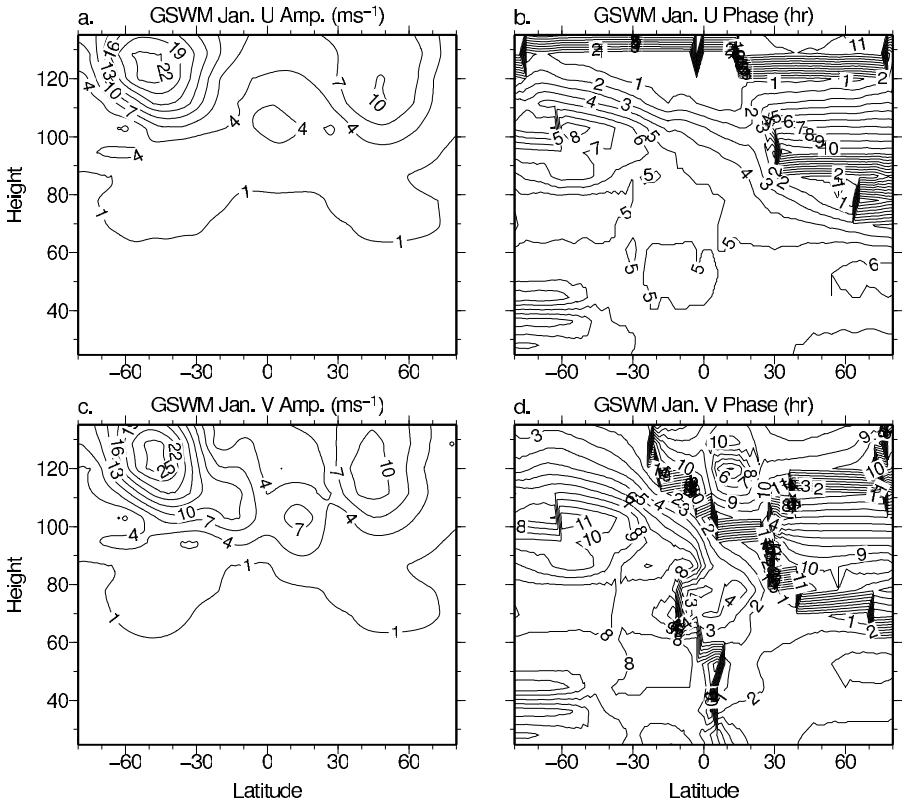

Figure 5. Same as Figure 4, except for the migrating semidiurnal lunar tide simulated by the GSWM.

with TIMED/SABER temperature observations of the semidiurnal lunar tide in the MLT (J. M. Forbes, personal communication, 2012). We thus believe that the GSWM overestimates the peak amplitude of the semidiurnal lunar tide. The height of the peak simulated by the GSWM is also roughly 10 km higher than the WACCM results. Although we are unsure as to the reason for the height discrepancy between the GSWM and WACCM, we believe that it may be related to the considerably different treatment of gravity waves and dissipation in the MLT between the two models. While the GSWM uses an effective Rayleigh friction for gravity wave drag, the WACCM incorporates a more comprehensive treatment of gravity waves. This is a significant difference between the two models and is likely to contribute to some of the differences in the lunar tide in GSWM and WACCM.

[18] To more clearly illustrate the seasonal behavior of the semidiurnal lunar tide in the MLT, Figures 8a–8d present the daily tidal amplitude as a function of latitude at fixed heights of 90 km, 95 km, 105 km, and 125 km, respectively. The annual variation of the lunar tide is dominated by two time periods of significantly enhanced tidal amplitude. The maxima occur between December and January, and also during June to August. The maximum that occurs around the December solstice is, however, observed to be slightly larger. At higher altitudes, the maxima around December solstice is also more symmetric in latitude. We note that the seasonal asymmetry, with larger amplitudes and a more latitudinally symmetric structure around December solstice may be of considerable importance with regards to producing the observed enhancement in the lunar tide in the ionosphere around December solstice [e.g., *Matsushita*, 1967]. It is also apparent from Figure 8 that at a fixed height, the maximum generally occurs at lower altitudes in the winter hemisphere, while at higher altitudes the maximum is observed in the summer hemisphere.

[19] To facilitate comparison of the present results with prior observations and model results, monthly average amplitudes of the semidiurnal lunar tide in zonal wind for different fixed latitudes and heights are presented in Figure 9. We first compare the present results with those from the model of *Vial and Forbes* [1994] at 90 km and 35°N and 35°S latitude. The seasonal variation at 35°S is generally consistent between these two models, although the WACCM amplitudes are 1.0–1.5 m s^{-1} smaller. At 35°N, there is a significant discrepancy between these two models during Northern Hemisphere summer. During this time period, the semidiurnal lunar tide at 35°N is significantly smaller in our simulations compared with results from the *Vial and Forbes* [1994] model. This difference is thought to be related to differences in the forcing of the lunar tide in these two models as well as the background atmosphere assumed in *Vial and Forbes* [1994]. It may also be related to the cold-pole bias in the WACCM, which could influence the global propagation of the lunar tide into the MLT. We will discuss the cold-pole bias and its possible influence on the results in more detail below.

[20] The WACCM simulations are also generally consistent with prior observations of the semidiurnal lunar tide in the MLT. At Poker Flat (66°N) zonal wind lunar tide observations at 90 km reveal a predominantly semiannual

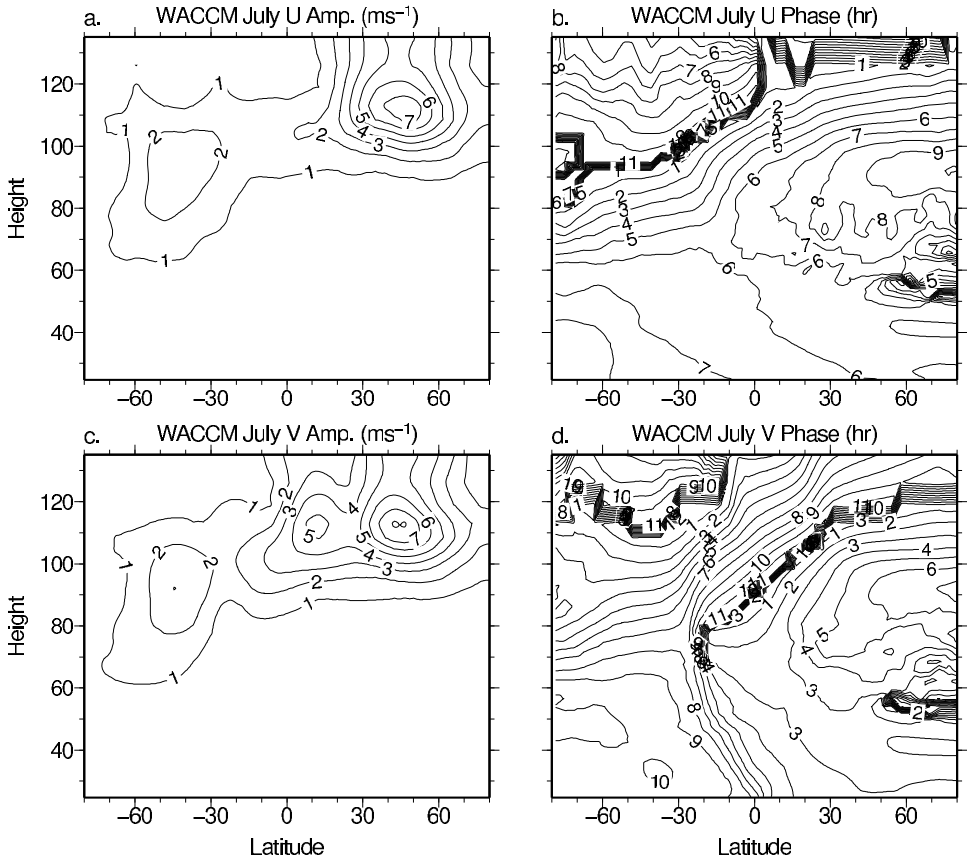

Figure 6. Migrating semidiurnal lunar tide (a) amplitude in zonal neutral wind, (b) phase in zonal neutral wind, (c) amplitude in meridional neutral wind, and (d) phase in meridional neutral wind. Results are for WACCM simulations during July.

variation with maxima around March and September [*Stening et al.*, 1990]. As shown in Figure 9, the WACCM results at 66°N show a broad maximum between July and October, but lack a second maximum around March. The observations at Poker Flat reveal lunar tide amplitudes of $\sim$5 ms^{-1} near March and September equinox, and these are considerably larger than the WACCM simulations. The observations are, however, only based on a single year of measurements, and it is therefore possible that the large difference between the observations and WACCM simulations is partly due to an exceptionally large lunar tide during the time of the observations. *Stening et al.* [1987] presented results for the semidiurnal lunar tide at Saskatoon, Canada. Comparison of their Figure 4 with the WACCM simulation results at 52°N and 95 km shows good agreement throughout most of the year, with the exception being around January and February. The observations show a significantly larger lunar tide during these months compared to the WACCM simulations. It is considered a strong possibility that this difference is related to inter-annual variability in the lunar tide, which can be particularly large during Northern Hemisphere winter due to sudden stratospheric warmings (SSWs) [*Stening et al.*, 1997a; Pedatella et al., submitted manuscript, 2012]. In the equatorial region, observations at Christmas Island reveal a lunar tide that is nearly constant throughout the year [*Stening et al.*, 1997b]. This is in contrast to the WACCM simulated lunar tide at 2°N and 90 km, which shows a clear annual variation with the maximum tidal amplitude occurring during Northern Hemisphere winter months. We further compare our simulation results at 44°S and 90 km with observations at Christchurch presented by *Stening et al.* [1995]. Both the observations and WACCM simulations achieve peak amplitudes in June to August, with a smaller, secondary, maxima occurring between December and February. However, the amplitudes in our simulations are again lower than what is seen in the observations. Based on these comparisons, the amplitude of lunar tide in the WACCM appears to be on average smaller than the observed amplitudes. However, it should be noted that the WACCM results are based on the 10-year climatological average while the aforementioned observations are often based on limited observations covering only a few years at best. Due to inter-annual variability a certain amount of phase cancelation occurs, and this tends to reduce the lunar tide amplitudes in the 10-year climatological average results that we present. As an example, amplitudes of the lunar semidiurnal tide for individual years (not shown) regularly reach $\sim$3−4 ms^{-1} at Poker Flat (66°N, 90 km) and $\sim$4−5 ms^{-1} at Saskatoon (52°N, 95 km). The amplitudes for individual years are thus more consistent with the observed amplitudes, indicating that the lower amplitudes in the climatological average results that we present are due in part to inter-annual variability.

[21] Although the overall agreement between the WACCM simulations and prior modeling results and observations is

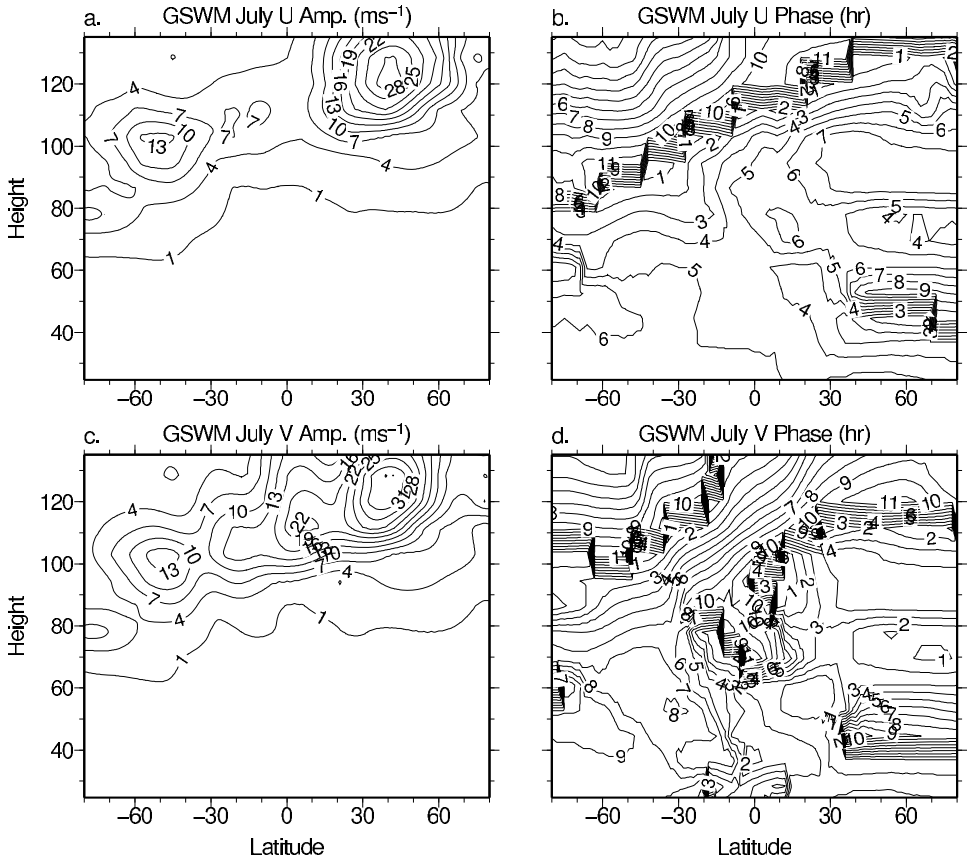

Figure 7. Same as Figure 6, except for the migrating semidiurnal lunar tide simulated by the GSWM.

generally good, there are some differences as previously discussed. Deficiencies in prior models, especially with regard to the assumed background atmospheric condition, along with the limited number of available observations in the MLT are likely to contribute to a portion of this disagreement. However, there are some shortcomings to the present WACCM simulations which may also influence our results. First, as previously discussed, we have neglected certain aspects of the lunar tidal forcing. Incorporating a more complex lunar tidal forcing that includes longitudinal varying ocean tides is anticipated to have a significant contribution in terms of improving the spatial variability of the lunar tide in our simulations. However, it is expected that this would have a relatively minor, if any, impact on the semidiurnal migrating lunar tide, which is by far the dominate tidal component. Another notable shortcoming in the present simulations is that the WACCM eastward winds in the Southern Hemisphere stratosphere are known to be too large during Southern Hemisphere winter months. This is due to the cold-pole bias that is a common problem among chemistry-climate models [*Austin et al.*, 2003]. Since the propagation of the lunar tide is sensitive to the background atmosphere, we believe that this will have an influence on our results. It is considered a possibility that this is responsible for the lower peak height of the semidiurnal lunar tide in the Southern Hemisphere during July (Figures 6 and 7). The cold-pole bias in the WACCM may also be responsible for the weaker lunar tide in our simulations during July to September in comparison with observations and prior model results.

4. Summary and Conclusions

[22] In the present paper we present the climatology of the atmospheric semidiurnal lunar tide based on the WACCM simulations. The atmospheric lunar tide is incorporated into the WACCM through inclusion of an additional forcing term that accounts for the M2 lunar potential, solid Earth tide, and migrating semidiurnal ocean tide. Our simulations show that the migrating semidiurnal lunar tide in surface pressure obtains maximum amplitudes at low-latitudes during Northern Hemisphere summer months. A significant phase change occurs between December and February in the simulation results. The consistency of the seasonal variations of the amplitude and phase of the migrating semidiurnal lunar tide in surface pressure with prior observations and model results validates our simulation results. The WACCM simulations also reproduce some of the longitudinal variability of the lunar tide in surface pressure, despite the fact that we only include a longitudinally invariant forcing.

[23] We have further established the climatological behavior of the lunar tide in the MLT based on the WACCM simulations. The WACCM results reveal that the migrating semidiurnal lunar tide achieves peak amplitudes of ~5–10 m s^{-1} in zonal and meridional neutral winds. The latitude and seasonal variation of the migrating semidiurnal tide in the WACCM is similar to results from the GSWM; however, the

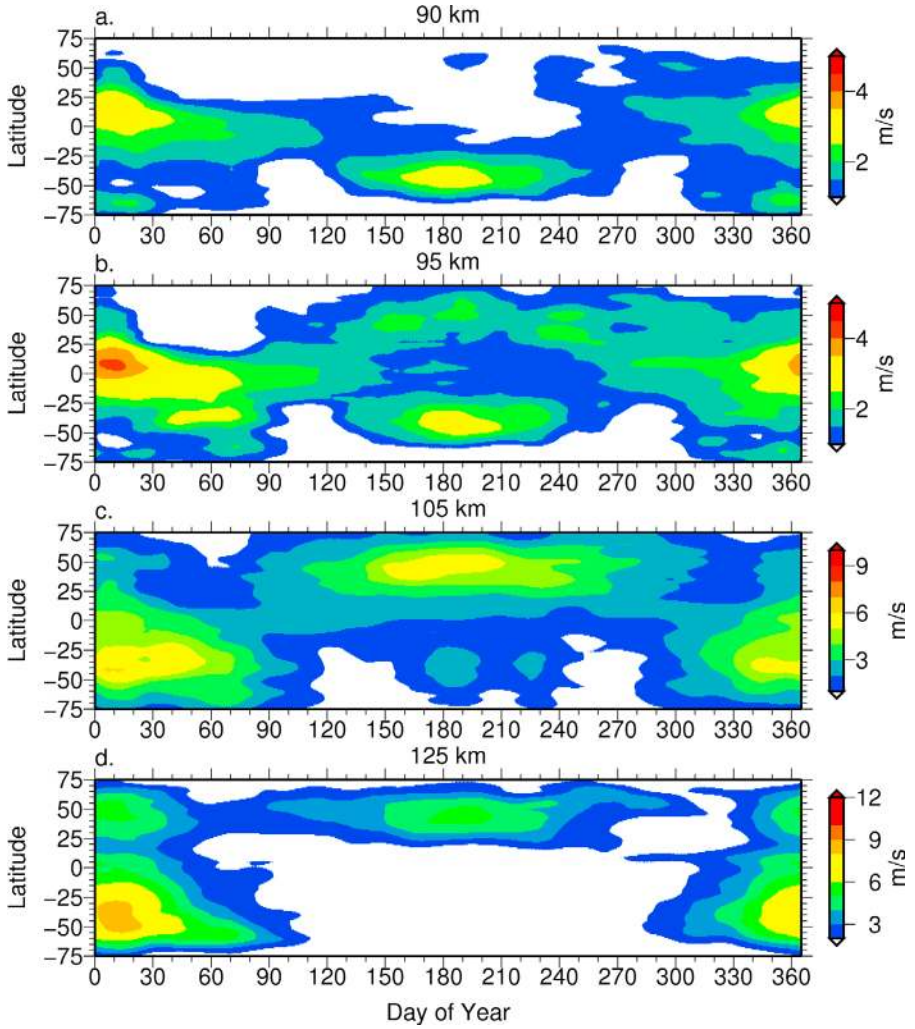

Figure 8. Seasonal and latitudinal variability of the migrating semidiurnal lunar tide amplitude in zonal neutral wind at (a) 90 km, (b) 95 km, (c) 105 km, and (d) 125 km.

peak amplitudes are 2–3 times larger in the GSWM. The difference between the GSWM and WACCM results is attributed primarily to different treatment of gravity waves between these two models. The WACCM simulations reveal maximum amplitudes in the MLT around December and June solstices. A hemispheric asymmetry is also observed with larger amplitudes occurring in the summer hemisphere. In general, the WACCM climatology of the semidiurnal lunar tide in the MLT is consistent with prior observations and modeling results; however, there are some differences. The largest difference between our simulation results and prior observations and numerical models is that the WACCM simulated lunar tide amplitudes are too small between July and September. This is thought to be related to the cold-pole bias, which is a known deficiency of the WACCM, and is likely to influence the propagation of the lunar tide into the MLT.

[24] Last, we note that although there are some shortcomings to the WACCM simulations of the lunar tide discussed in the present study, simulating the lunar tide in a non-linear, chaotic model such as the WACCM offers many advantages. Prior simulations of the atmospheric lunar tide have relied on linear, steady state numerical models, and the simulated lunar tide is significantly influenced by the assumed background atmosphere in these models. While such an approach is useful for studying the climatological

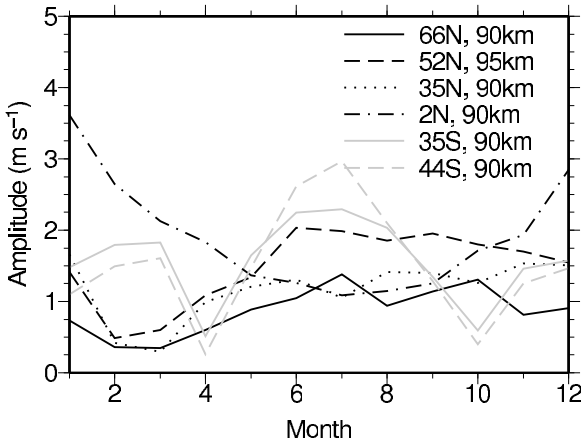

Figure 9. Monthly average amplitudes of the migrating semidiurnal lunar tide in zonal wind. Results are shown for selected latitudes and heights as indicated on the figure.

behavior of the lunar tide, it inhibits the investigation of dynamical processes which may significantly influence the atmospheric lunar tide. In particular, the investigation of short-term variability in the semidiurnal lunar tide is difficult in linear steady state tidal models. In a follow-on study (Pedatella et al., submitted manuscript, 2012), we make use of the chaotic nature of the WACCM to investigate short-term variability in the semidiurnal lunar tide.

[25] **Acknowledgments.** We thank J. M. Forbes, M. E. Hagan, and X. Zhang for their discussions and assistance with the GSWM. The National Center for Atmospheric Research is sponsored by the National Science Foundation. H.-L. Liu acknowledges support from NSF CEDAR grant ATM-0836386, NASA LWS Strategic Capability grant NNX09AJ83G, and NASA LWS grant NNX08AQ91G.

[26] Robert Lysak thanks the reviewers for their assistance in evaluating this paper.

References

Aso, T., T. Nonoyama, and S. Kato (1981), Numerical simulation of semidiurnal atmospheric tides, *J. Geophys. Res.*, *86*(A13), 11,388–11,400, doi:10.1029/JA086iA13p11388.

Austin, J., et al. (2003), Uncertainties and assessments of chemistry-climate models of the stratosphere, *Atmos. Chem. Phys.*, *3*, 1–27.

Chapman, S., and R. S. Lindzen (1970), *Atmospheric Tides*, 201 pp., D. Reidel, Norwell, Mass.

Chapman, S., and K. K. Tschu (1948), The lunar atmospheric tide at twenty-seven stations widely distributed over the globe, *Proc. R. Soc. London*, *195*, 310–323.

Fejer, B. G., M. E. Olson, J. L. Chau, C. Stolle, H. Lühr, L. P. Goncharenko, K. Yumoto, and T. Nagatsuma (2010), Lunar-dependent equatorial ionospheric electrodynamic effects during sudden stratospheric warmings, *J. Geophys. Res.*, *115*, A00G03, doi:10.1029/2010JA015273.

Forbes, J. M. (1982a) Atmospheric tides: 1. Model description and results for the solar diurnal component, *J. Geophys. Res.*, *87*(A7), 5222–5240, doi:10.1029/JA087iA07p05222.

Forbes, J. M. (1982b) Atmospheric tides: 2. The solar and lunar semidiurnal components, *J. Geophys. Res.*, *87*(A7), 5241–5252, doi:10.1029/JA087iA07p05241.

Garcia, R. R., D. R. Marsh, D. E. Kinnison, B. A. Boville, and F. Sassi (2007), Simulation of secular trends in the middle atmosphere, 1950–2003, *J. Geophys. Res.*, *112*, D09301, doi:10.1029/2006JD007485.

Geller, M. A. (1970), An investigation of the lunar semidiurnal tide in the atmosphere, *J. Atmos. Sci.*, *27*, 202–218.

Hagan, M. E., and J. M. Forbes (2002), Migrating and nonmigrating diurnal tides in the middle and upper atmosphere excited by tropospheric latent heat release, *J. Geophys. Res.*, *107*(D24), 4754, doi:10.1029/2001JD001236.

Hagan, M. E., J. M. Forbes, and F. Vial (1993), A numerical investigation of the propagation of the quasi 2-day wave into the lower thermosphere, *J. Geophys. Res.*, *98*, 23,193–23,205.

Hagan, M. E., J. M. Forbes, and F. Vial (1995), On modeling migrating solar tides, *Geophys. Res. Lett.*, *22*, 893–896.

Hagan, M. E., M. D. Burrage, J. M. Forbes, J. Hackney, W. J. Randel, and X. Zhang (1999), GSWM-98: Results for migrating solar tides, *J. Geophys. Res.*, *104*, 6813–6828.

Haurwitz, B., and A. D. Cowley (1969), The lunar barometric tide, its global distribution and annual variation, *Pure Appl. Geophys.*, *77*, 122–150.

Hollingsworth, A. (1971), The effect of ocean and Earth tides on the semidiurnal lunar air tide, *J. Atmos. Sci.*, *28*, 1021–1044.

Lindzen, R. S., and S. S. Hong (1974), Effects of mean winds and horizontal temperature gradients on solar and lunar semidiurnal tides in the atmosphere, *J. Atmos. Sci.*, *31*, 1421–1446.

Matsushita, S. (1967), Lunar tides in the ionosphere, *Handb. Phys.*, *49*(2), 547–602.

Park, J., H. Lühr, M. Kunze, B. G. Fejer, and K. W. Min (2012), Effect of sudden stratospheric warming on lunar tidal modulation of the equatorial electrojet, *J. Geophys. Res.*, *117*, A03306, doi:10.1029/2011JA017351.

Ray, R. D. (1999), A global ocean tide model from TOPEX/POSEIDON altimetry: GOT99.2, *NASA Tech. Memo.*, *NASA TM-1999-209478*, 59 pp.

Sabine, E. (1847), On the lunar atmospheric tide at St. Helena, *Philos. Trans. R. Soc. London*, *137*, 45–50.

Sandford, D. J., H. G. Muller, and N. J. Mitchell (2006), Observations of lunar tides in the mesosphere and lower thermosphere at Arctic and middle latitudes, *Atmos. Chem. Phys.*, *6*, 4117–4127.

Stening, R. J., and C. Jacobi (2001), Lunar tidal winds in the upper atmosphere over Collm, *Ann. Geophys.*, *18*, 1645–1650.

Stening, R. J., and R. A. Vincent (1989), A measurement of lunar tides in the mesosphere at Adelaide, *J. Geophys. Res.*, *94*, 10,121–10,129.

Stening, R. J., C. E. Meek, and A. H. Manson (1987), Lunar tidal winds measured in the upper atmosphere (68–105 km) at Saskatoon, Canada, *J. Atmos. Sci.*, *44*, 1143–1151.

Stening, R. J., S. K. Avery, and D. Tetenbaum (1990), Observations of lunar tides in upper atmosphere winds at Poker Flat, Alaska, *J. Atmos. Terr. Phys.*, *52*, 715–721.

Stening, R. J., A. H. Manson, C. E. Meek, and R. A. Vincent (1994), Lunar tidal winds at Adelaide and Saskatoon at 80 to 100 km heights, 1985–1990, *J. Geophys. Res.*, *99*, 13,273–13,280.

Stening, R. J., K. Fleming, and G. Fraser (1995), Upper atmosphere semidiurnal tides at Christchurch (44°S) and Scott Base (78°S), *J. Atmos. Sol. Terr. Phys.*, *57*, 857–869.

Stening, R. J., J. M. Forbes, M. E. Hagan, and A. D. Richmond (1997a), Experiments with a lunar atmospheric tidal model, *J. Geophys. Res.*, *102*(D12), 13,465–13,471, doi:10.1029/97JD00778.

Stening, R. J., D. M. Schlapp, and R. A. Vincent (1997b), Lunar tides in the mesosphere over Christmas Island (2°N, 203°E), *J. Geophys. Res.*, *102*(D22), 26,239–26,245, doi:10.1029/97JD00898.

Stening, R. J., T. Tsuda, and T. Nakamura (2003), Lunar tidal winds in the upper atmosphere over Jakarta, *J. Geophys. Res.*, *108*(A5), 1192, doi:10.1029/2002JA009528.

Tsuda, T., J. Tanii, T. Aso, and S. Kato (1981), Lunar tides at meteor heights, *Geophys. Res. Lett.*, *8*(3), 191–194.

Vial, F., and J. M. Forbes (1994), Monthly simulations of the lunar semidiurnal tide, *J. Atmos. Terr. Phys.*, *56*, 1591–1607.

Yamazaki, Y., A. D. Richmond, and K. Yumoto (2012), Stratospheric warmings and the geomagnetic lunar tide: 1958–2007, *J. Geophys. Res.*, *117*, A04301, doi:10.1029/2012JA017514.